

# Hot Holographic 2-flavor Quark Star

---

**Le-Feng Chen,<sup>a</sup> Jing-Yi Wu,<sup>b,1</sup> Hao Feng,<sup>a</sup> Tian-Shun Chen,<sup>a</sup> and Kilar Zhang<sup>a,c,d,1</sup>**

<sup>a</sup>*Department of Physics and Institute for Quantum Science and Technology, Shanghai University, Shanghai 200444, China*

<sup>b</sup>*School of Astronomy and Space Science, University of Chinese Academy of Sciences (UCAS), Beijing 100049, China*

<sup>c</sup>*Shanghai Key Lab for Astrophysics, Shanghai 200234, China*

<sup>d</sup>*Shanghai Key Laboratory of High Temperature Superconductors, Shanghai 200444, China*

*E-mail:* [clf@shu.edu.cn](mailto:clf@shu.edu.cn), [wujingyi222@mailsucas.ac.cn](mailto:wujingyi222@mailsucas.ac.cn),  
[fenghaozi@shu.edu.cn](mailto:fenghaozi@shu.edu.cn), [cts2003912@shu.edu.cn](mailto:cts2003912@shu.edu.cn), [kilar@shu.edu.cn](mailto:kilar@shu.edu.cn)

ABSTRACT: Applying the holographic 2-flavor Einstein-Maxwell-dilaton model, the parameters of which fixed by lattice QCD, we extract the equations of state for hot quark-gluon plasma around the critical point at  $T = 182$  MeV, and have corresponding quark star cores constructed. By further adding hadron shells, the mass range of the whole stars spans from 2 to 17 solar masses, with the maximum compactness around 0.15. This result allows them to be black hole mimickers and candidates for gap events. The I-Love-Q-C relations are also analyzed, which show consistency with the neutron star cases when the discontinuity at the quark-hadron interface is not large. Besides, we illustrate the full parameter maps of the energy density and pressure as functions of the temperature and chemical potential, and discuss the constant thermal conductivity case supposing a heat source inside.

---

<sup>1</sup>Corresponding author.

---

## Contents

<b>1</b>	<b>Introduction</b>	<b>1</b>
<b>2</b>	<b>Holographic 2-flavor QCD Model</b>	<b>3</b>
<b>3</b>	<b>Hot Quark Stars and Their I-Love-Q-C Relations</b>	<b>5</b>
<b>4</b>	<b>More Discussions on the <math>\epsilon</math> and <math>p</math> Parameter Space</b>	<b>12</b>
<b>5</b>	<b>Conclusions</b>	<b>16</b>

---

## 1 Introduction

How to get bare quarks has been a long challenge, since the extreme conditions is almost impossible to realize on the earth. A possible solution may lie in compact stars, like in the cores of neutron stars (NS).

Gravitational Waves (GW) offer us a brand new way to detect NS since the summer of 2017 [1–3], deciphering the information of masses and tidal deformations [4]. Together with the traditional electromagnetic (EM) observation apparatus like NICER [5], we can narrow the windows and place constraints on the NS equation of state (EoS), excluding many EoS candidates. However, only observations are far from enough to break the degeneracy, and theoretical derivations are needed.

Unfortunately, theoretically obtaining the exact EoS for NS is still an open question, not to say that for quark stars (QS). Those require highly non-perturbative quantum chromodynamics (QCD), beyond the current analysis and calculation power. At this stage, holographic methods [6, 7] provide hopeful approaches to extract the EoS. Two major holographic QCD models originating from string theory, one from brane constructions, and the other called Einstein-Maxwell-dilaton (EMD) [8] model, could both lead to competitive EoS candidates.

For brane constructions, as a top-down model, applying D4/D8 brane configurations, namely Witten-Sakai-Sugimoto (WSS) model [9–11], one can extract NS EoS. On the other hand, D3/D7 configurations can lead to QS EoS.

For QS itself, there are also two scenarios. Low or zero temperature and high density lead to quark matter, but most of the current models (including D3/D7 model) [12–16] do not favor the existence of quark cores, as the stars constructed are unstable. As some exceptions, studies [17–21] have found that stable NS can form with cold quark cores. High temperature and relatively lower density result in quark-gluon plasma, which may form a new type of star [22] rather than NS. The EoS can be provided by EMD model, which has the advantage that the coefficients are fixed by comparing with lattice QCD at zero

chemical potential [23, 24]. The compactness may will be lower, but the total mass will be much larger. We considered 2 + 1-flavor case in [22], and now we discuss the 2-flavor case.

There are two major differences from the last work. First is of course the change of flavors. Constraining to only up and down quarks are in some sense more realistic. Secondly, we now show the whole parameter spaces for  $\epsilon$  and  $p$  as functions of  $T$  and  $\mu$ , and discuss the special curves under constant thermal conductivity in addition.

We end up with hot and massive QS, the maximum masses of which ranging from 15 to 17  $M_{\odot}$ , much larger than NS, though lower compared to their 2 + 1-flavor counterparts with 23 to 30  $M_{\odot}$  in [22]. This property enable them to mimic black holes (BH) rather than NS.

For the formation and lifetime of such high temperature stars, similar questions arise like the cases in [22]. In both the early universe and core-collapse supernovae, extreme conditions may generate temperatures sufficient for quark-gluon plasma formation. While supernovae can reach as high as 30-50 MeV [25, 26] in the literature, we suggest that certain extreme explosions could attain temperatures several times higher to more than 182 MeV, potentially creating hot QS. While hot QS may predict rapid collapse into NS and subsequently BH due to intense thermal radiation, the models in this paper are dealing with a stratified structure featuring a quark-phase core enveloped by neutron-rich matter. Crucially, strong radiation reflection at the phase transition boundary may significantly reduce energy leakage from the quark core, thereby extending the stellar lifespan. Detailed investigation of this interface dynamics and its observational implications will be addressed in future work.

In order to analyze the ability of detections, we calculate the universal relations across the moment of inertia (I), the tidal deformability (Love), and the quadrupole moment (Q) and the compactness (C), which is also called the I-Love-Q-C relations. The relations have been found to be independent on most models whether the EoS are continuous [27–34] or with small discontinuity [35–39]. As BH mimickers, the stars are distinguishable by comparing the masses with the detection results of NS. Furthermore, the stars can be differentiated with BH by characteristic wave forms, and further the non-zero tidal love number (TLN) in contrast to the zero TLN of BH in general relativity. The deviations of the I-Love-Q-C relations for different models are also effective in observations. Moreover, the thermal radiation emitted by such high-temperature stars provides traditional methods for their detection.

This paper is organized as follows. Section 1 is the introduction, and section 2 summarizes the way to extract EoS from holographic 2-flavor EMD model. Section 3 shows the QS constructed and analyze their I-Love-Q-C Relations. We discuss more on the full parameter space of  $\epsilon$  and  $p$ , and consider the constant thermal conductivity case in section 4. We conclude in section 5.

## 2 Holographic 2-flavor QCD Model

We conduct research within the EMD theoretical framework in five-dimensional space. The action of the system is represented as:

$$S = \frac{1}{2\kappa_N^2} \int d^5x \sqrt{-g} \left[ R - \frac{1}{2} \nabla_\mu \phi \nabla^\mu \phi - \frac{Z(\phi)}{4} F_{\mu\nu} F^{\mu\nu} - U(\phi) \right], \quad (2.1)$$

where  $\kappa_N$  represents the effective Newton constant,  $\phi$  is a scalar field called dilaton, which breaks conformal symmetry,  $F_{\mu\nu}$  is the field strength tensor of the U(1) gauge field, and  $g$  denotes the determinant of the five-dimensional spacetime metric tensor,  $R$  is the Ricci scalar curvature. The scalar potential  $U(\phi)$  and the gauge coupling function  $Z(\phi)$ , are chosen to reproduce key features of 2-flavor lattice QCD at zero chemical potential. Based on the work of [40], we adopt the following forms:

$$\begin{aligned} U(\phi) &= -12 \cosh[c_1 \phi] + (6c_1^2 - \frac{3}{2})\phi^2 + c_2 \phi^6, \\ Z(\phi) &= \frac{\text{sech}[c_4 \phi^3]}{1 + c_3} + \frac{c_3}{1 + c_3} e^{-c_5 \phi}. \end{aligned} \quad (2.2)$$

As established by lattice data in [40], the parameters  $\kappa_N$  and  $c_i$  are determined as the following values:  $\kappa_N^2 = 2\pi(3.72)$ ,  $c_1 = 0.7100$ ,  $c_2 = 0.0002$ ,  $c_3 = 0.530$ ,  $c_4 = 0.085$ , and  $c_5 = 30$ .

The metric form of a five-dimensional AdS black hole with scalar hair is as follows

$$ds^2 = -f(r)e^{-\eta(r)} dt^2 + \frac{dr^2}{f(r)} + r^2(dx^2 + dy^2 + dz^2), \quad (2.3)$$

and

$$\phi = \phi(r), \quad A_t = A_t(r). \quad (2.4)$$

where  $f(r)$  and  $\eta(r)$  are all functions of  $r$ , and  $A_t$  is the t-component of the gauge field.

The temperature  $T$  and entropy density  $s$  can both be obtained from the horizon

$$T = \frac{1}{4\pi} f'(r_h) e^{-\eta(r_h)/2}, \quad s = \frac{2\pi}{\kappa_N^2} r_h^3, \quad (2.5)$$

where  $r_h$  is the horizon radius.

Through the calculation method in [23], the specific form of energy density  $\epsilon$  and pressure  $p$  can be obtained

$$\begin{aligned} \epsilon &= \frac{1}{2\kappa_N^2} \left( -3f_v + \phi_s \phi_v + \frac{1 + 48b}{48} \phi_s^4 \right), \\ p &= \frac{1}{2\kappa_N^2} \left( -f_v + \phi_s \phi_v + \frac{3 - 48b - 8c_1^4}{48} \phi_s^4 \right), \end{aligned} \quad (2.6)$$

where  $f_v, \phi_s, \phi_v$  are the parameters in the asymptotic expansion of the metric function on the AdS boundary, and  $b = -0.25707$  is the result from holographic renormalization. The  $\phi_s$  originate from the asymptotic expansion of scalar fields, and their non-zero values

break the conformal symmetry. Additionally, the value of  $\phi_s = 1.227$  GeV [40] can be fixed through lattice QCD.

To obtain the mass and the radius of the star through solving Tolman-Oppenheimer-Volkoff (TOV) equations with the EoS, we need to convert the usual QCD units [MeV<sup>4</sup>] into the so-called astronomical units  $r_\odot, \epsilon_\odot, p_\odot$ , with  $r_\odot = G_N M_\odot / c^2, \epsilon_\odot = M_\odot / r_\odot^3$ , and  $p_\odot = c^2 \epsilon_\odot$ ,

$$\epsilon_\odot = p_\odot = 6.60271 \times 10^{14} \text{ MeV}^4 = 3.14644 \times 10^5 \text{ MeV} \cdot \text{fm}^{-3}, \quad (2.7)$$

where we have taken  $c = G_N = 1$ .

In [40], they obtained the critical end point (CEP) of 2-flavor QCD ( $\mu = 219$  MeV,  $T = 182$  MeV). For simplified analysis, we selected five sets of data points around CEP, which are  $\mu/T = 1, \mu/T = 1.2033, \mu/T = 1.25, T = 182$  MeV and  $\mu = 219$  MeV, and performed fittings on these data, with the fitting results and data shown in Fig.1. The real EoS will be contained within this range, though complicated to get directly.

We must emphasize that, the blue data points in Fig.1 do not reach zero because we select the high-temperature quark-gluon plasma, in which case neither pressure nor temperature is zero.

The fitting results corresponding to different physical conditions are listed below:  $p_1, \epsilon_1$  for  $\mu/T = 1, p_2, \epsilon_2$  for  $\mu/T = 1.2033, p_3, \epsilon_3$  for  $\mu/T = 1.25, p_4, \epsilon_4$  for  $T = 182$  MeV,  $p_5, \epsilon_5$  for  $\mu = 219$  MeV.

$$\begin{aligned} \epsilon_1 &= 0.000501863 p_1^{0.315468} + 1.15292 p_1^{0.89651}, \\ p_1 &\in [3.0918 \times 10^{-8}, 7.3047 \times 10^{-6}], \\ \epsilon_1 &\in [2.1682 \times 10^{-6}, 4.066 \times 10^{-5}], \end{aligned} \quad (2.8)$$

$$\begin{aligned} \epsilon_2 &= 0.00139264 p_2^{0.375067} + 2.6989 p_2^{0.982421}, \\ p_2 &\in [2.627 \times 10^{-8}, 7.3045 \times 10^{-6}], \\ \epsilon_2 &\in [1.7023 \times 10^{-6}, 4.0658 \times 10^{-5}], \end{aligned} \quad (2.9)$$

$$\begin{aligned} \epsilon_3 &= 0.000928211 p_3^{0.349754} + 2.15744 p_3^{0.958067}, \\ p_3 &\in [2.3732 \times 10^{-8}, 7.35366 \times 10^{-6}], \\ \epsilon_3 &\in [1.6962 \times 10^{-6}, 4.08 \times 10^{-5}], \end{aligned} \quad (2.10)$$

$$\begin{aligned} \epsilon_4 &= 0.00117483 p_4^{0.350591} + 11.3855 p_4^{1.13679}, \\ p_4 &\in [2.61368 \times 10^{-8}, 1.1615 \times 10^{-5}], \\ \epsilon_4 &\in [2.1067 \times 10^{-6}, 4.9673 \times 10^{-5}], \end{aligned} \quad (2.11)$$

$$\begin{aligned} \epsilon_5 &= 0.001427 p_5^{0.378816} + 2.09627 p_5^{0.958741}, \\ p_5 &\in [2.60394 \times 10^{-8}, 6.97167 \times 10^{-6}], \\ \epsilon_5 &\in [1.5845 \times 10^{-6}, 3.967 \times 10^{-5}]. \end{aligned} \quad (2.12)$$

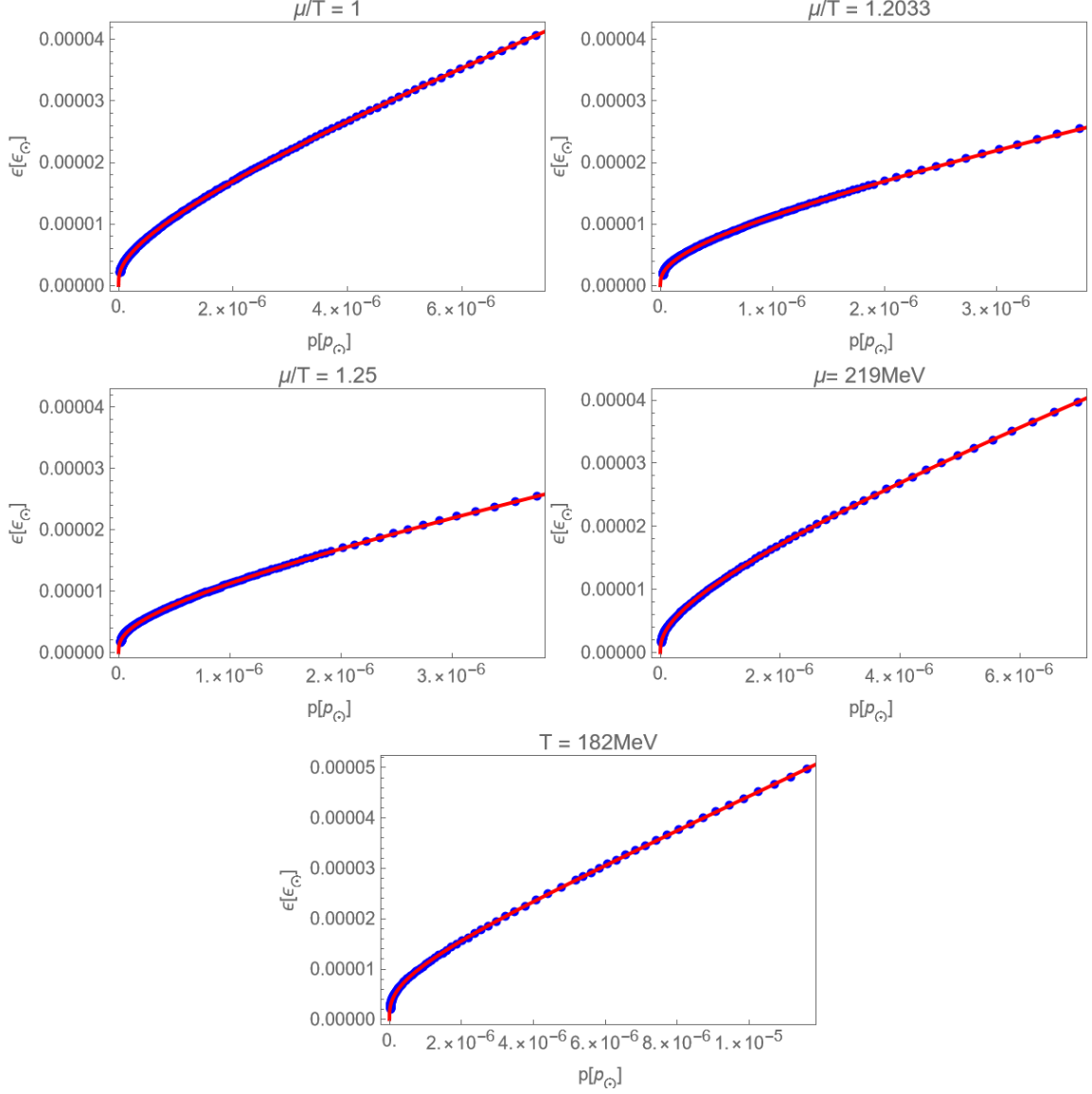


**Figure 1:** Energy-pressure data and fitted curves under five different  $T, \mu$  conditions. Blue points represent numerical data, and red lines are fitted curves. Here our data does not reach zero because this is high-temperature quark matter, which still maintains a certain pressure at the phase transition point.

The permissible fitting ranges for pressure ( $p$ ) and energy density ( $\epsilon$ ) in astrophysical units are constrained as follows: the minimum values correspond to the phase transition threshold, whereas the maximum values are determined by stellar stability requirements.

### 3 Hot Quark Stars and Their I-Love-Q-C Relations

Theoretically inferred models play a crucial role in supporting astrophysical observations by leveraging universal relations among key macroscopic properties of compact stars—namely,

I-Love-Q trio [27, 28]. These nearly EoS-independent relations enable the extraction of fundamental stellar parameters from gravitational wave and pulsar timing observations, providing a powerful tool for probing the internal structure and composition of compact objects, including NS and QS.

In Fig.2, we plot the mass-radius (M-R) curve and the I-Love-Q-C relations of the models in Eq.(2.8-2.12) with the calculation procedures in [28]. We plot the  $\epsilon$  and  $p$  with TOV units  $\epsilon_{\odot}$  and  $p_{\odot}$  while the I-Love-Q-C are dimensionless. We should note that as shown in Fig.1, the pressure of quark phase is nonzero, but for the simplest analysis, we extend the fitting of the models to  $p = 0$  as the surface condition required, so that the hadron shell share the same EoS curve (with a smooth phase transition), and we use the terminology "simple" to represent the models. For comparison, we plot the I-Love-Q-C relations for a single polytropic NS model

$$\epsilon_n = \kappa_n p^{\gamma_n}, \quad (3.1)$$

with the black dotted curve. Here  $\gamma_n$  is set to 0.5 as a typical reference and the corresponding  $\kappa_n = 0.09$ , which satisfies the constraint that the maximum mass of NS is about  $2.2 M_{\odot}$ , also the parameters used in [41]. From Fig.2, we observe that the maximum masses of the quark models can reach up to  $17 M_{\odot}$ . In sight of the panels of the I-Love-Q trio, we find the models still obey the universal relations, compared with the NS model. But for the curves about the compactness, the universality is broken. We regard the deviations as plausible because there exists differences between the unrealistic NS EoS and the realistic ones [28].

More realistically than the "simple" EoS cases, we introduce the "combined" cases: considering that the quark-gluon plasma cools down as it approaches the surface and eventually undergoes a phase transition, we connect the quark cores with the hadron (probably, neutron) shells at their respective minimum pressure. The hadron model we use is Eq.(3.1) with a fixed  $\gamma_n = 0.5$ . At the transition point, we set

$$\epsilon_n(p_t) = m \epsilon_q(p_t), \quad (3.2)$$

to illustrate the discontinuities. Here  $\epsilon_q$  is referred to the energy density of the quark cores and  $p_t$  represents the transition point. The parameter  $\kappa_n$  depends on the choice of  $m$ .

We plot the EoS, M-R relations and I-Love-Q-C relations for "combined" QS with  $m = 1, 1.2, 0.8$  and  $0.5$  in Fig.3-6 through the procedures for the two-layer models in [42]. In the panels for M-R relations, we show that the "combined" QS have more instable components (i.e. the higher radii parts of the stars) for the larger phase transitions while the stability judging methods can be seen in [43]. We should mention that the selection of the ranges of the central pressure  $p_0$ , which are the initial conditions when solving TOV equations to derive the mass and radius, are the same across all "combined" QS for the respective quark EoS. Through the trend of the instability with the phase transition, we can foresee the stars will not exist in the extreme circumstances. From the lower six panels, we observe that the I-Love-Q relations are valid for all the "combined" cases. The I-C, Love-C and Q-C curves obey the universality except for  $m = 0.5$  which may be induced by

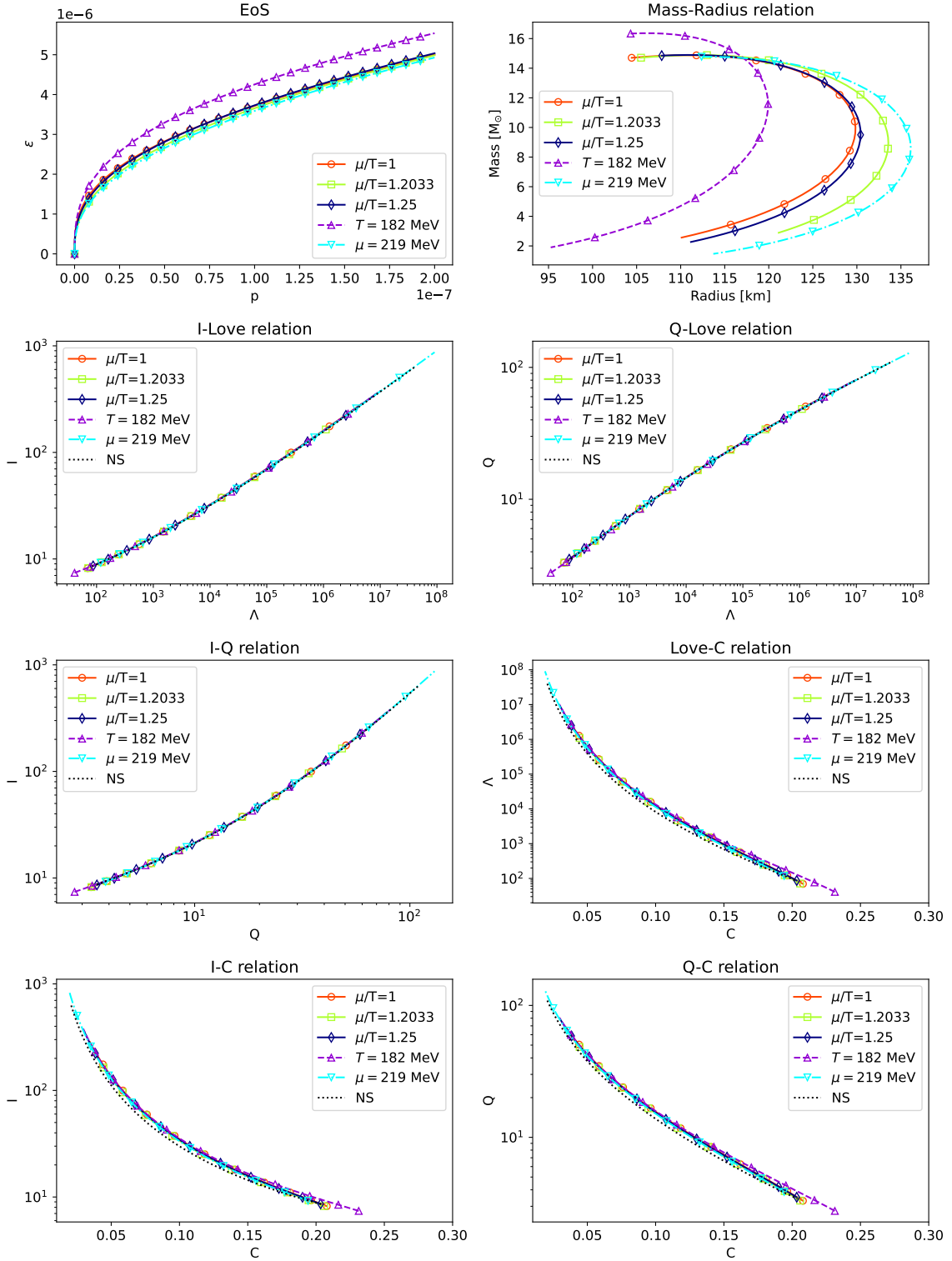


**Figure 2:** The EoS, M-R relation, and I-Love-Q-C relations for the "simple" QS are presented using various models described in Eq. (2.8–2.12). For comparison, the panels showing the I-Love-Q-C relations of a polytropic NS, given by  $\epsilon_n = 0.09p_n^{0.5}$ , is plotted with a black dotted line.



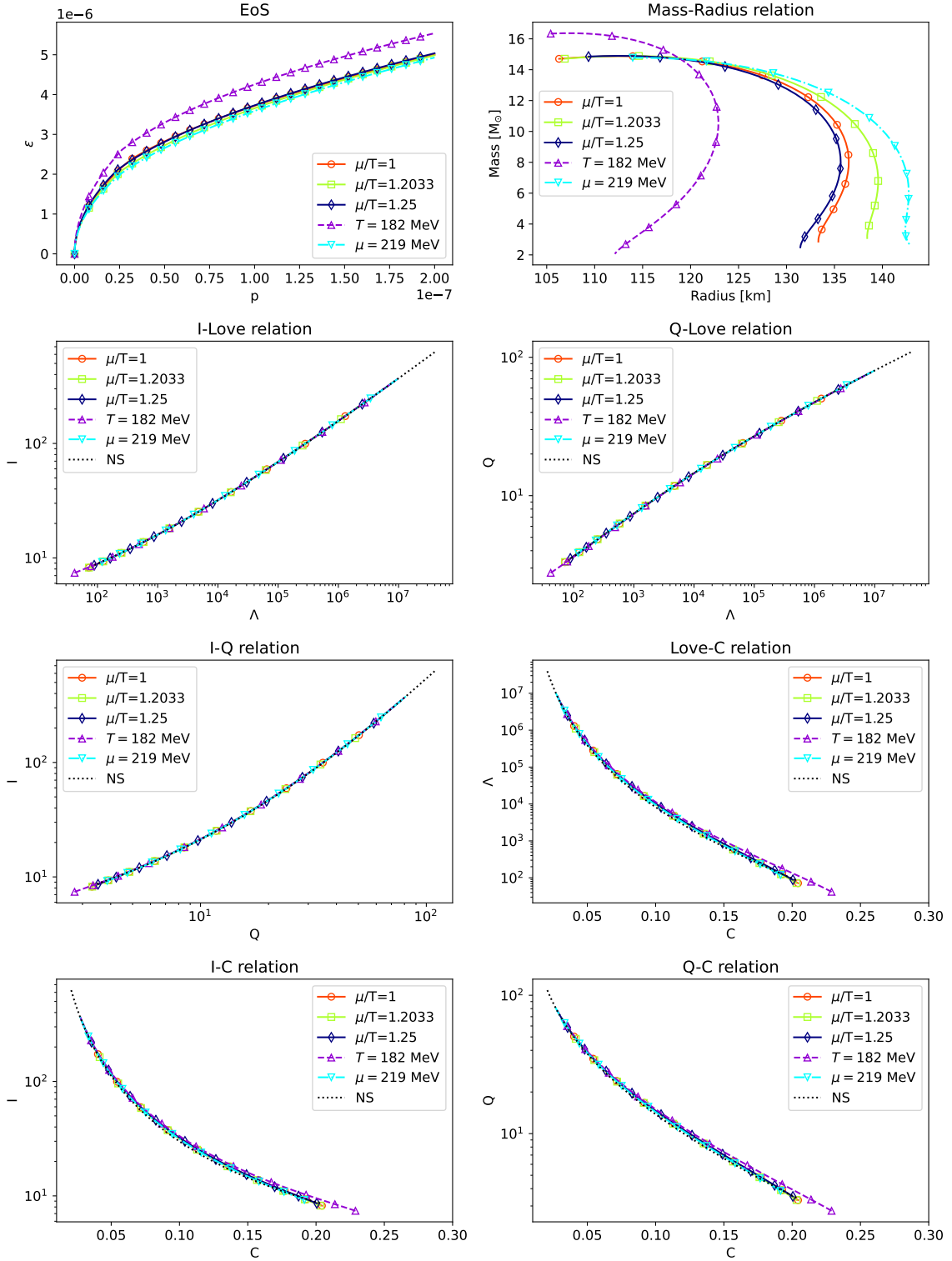


**Figure 3:** The EoS, M-R relation, and I-Love-Q-C relations for the "combined" QS consisting of quark cores and hadron shells with  $m = 1$  in Eq.(3.2). For comparison, the panels showing the I-Love-Q-C relations of a polytropic NS, given by  $\epsilon_n = 0.09p_n^{0.5}$ , is plotted with a black dotted line.

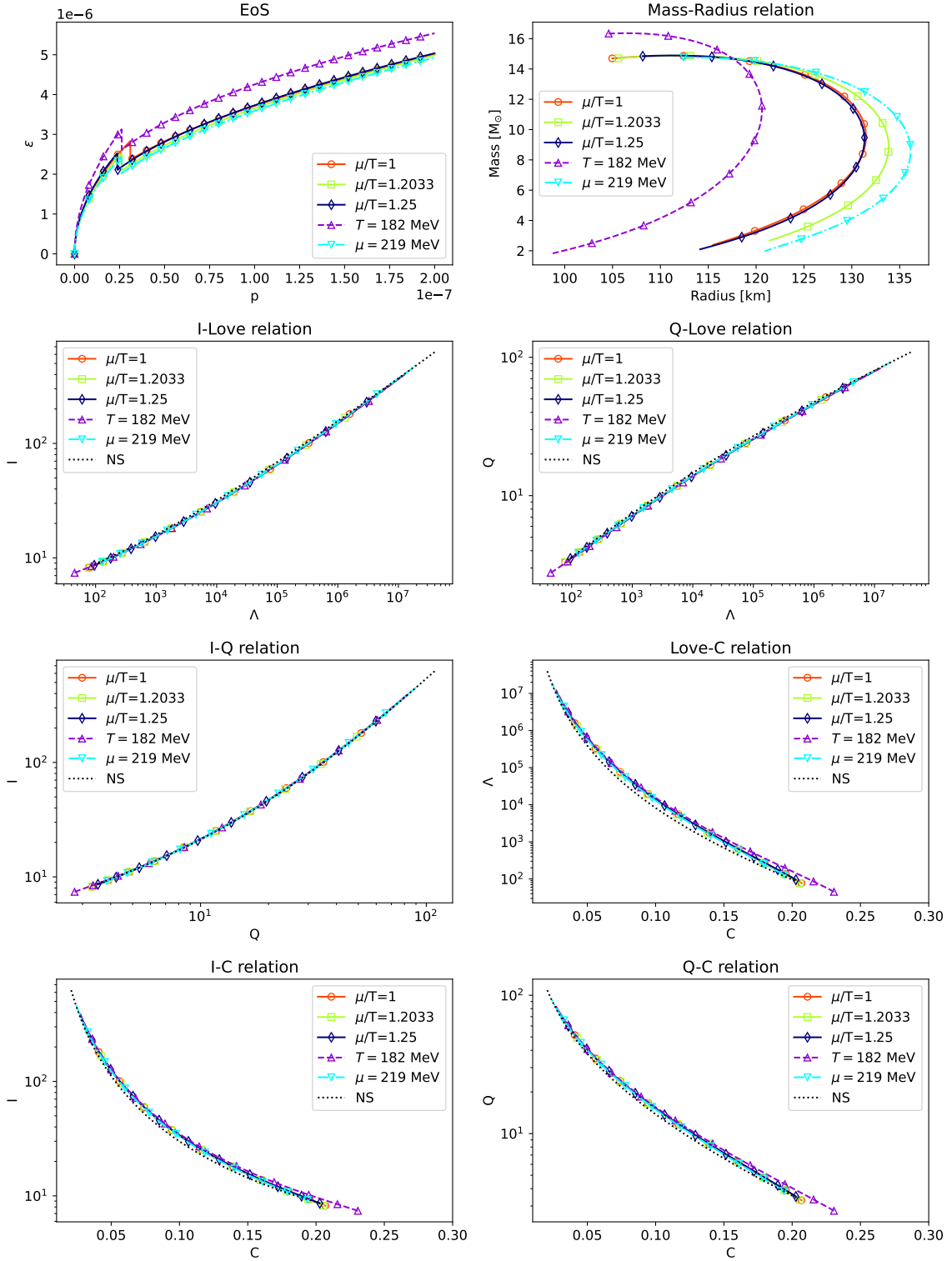


**Figure 4:** The EoS, M-R relation, and I-Love-Q-C relations for the "combined" QS consisting of quark cores and hadron shells with  $m = 1.2$  in Eq.(3.2). For comparison, the panels showing the I-Love-Q-C relations of a polytropic NS, given by  $\epsilon_n = 0.09p_n^{0.5}$ , is plotted with a black dotted line.

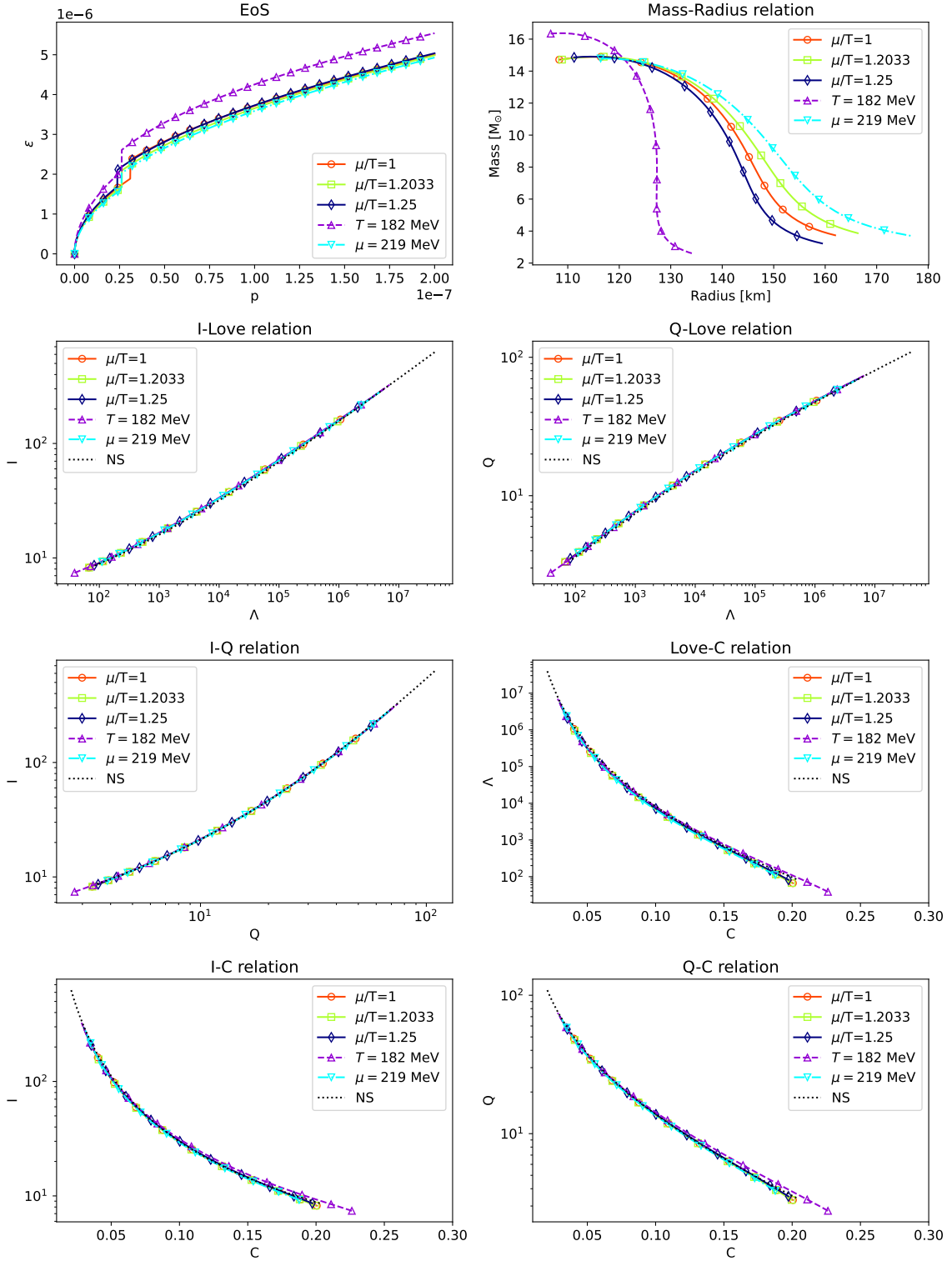


**Figure 5:** The EoS, M-R relation, and I-Love-Q-C relations for the "combined" QS consisting of quark cores and hadron shells with  $m = 0.8$  in Eq.(3.2). For comparison, the panels showing the I-Love-Q-C relations of a polytropic NS, given by  $\epsilon_n = 0.09\rho_n^{0.5}$ , is plotted with a black dotted line.

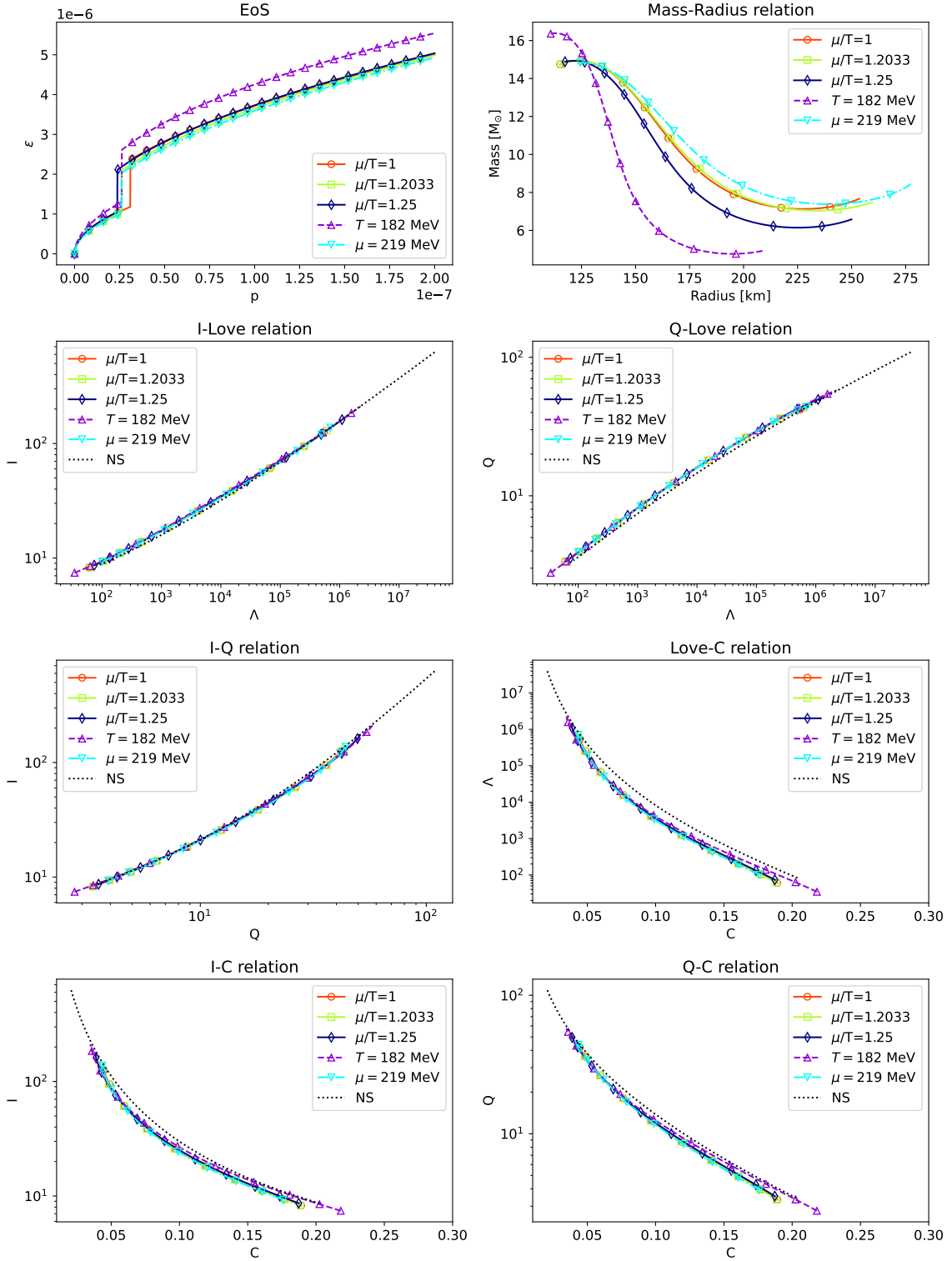


**Figure 6:** The EoS, M-R relation, and I-Love-Q-C relations for the "combined" QS consisting of quark cores and hadron shells with  $m = 0.5$  in Eq.(3.2). For comparison, the panels showing the I-Love-Q-C relations of a polytropic NS, given by  $\epsilon_n = 0.09\rho_n^{0.5}$ , is plotted with a black dotted line.

the larger phase transition. Compared with Fig.2, the relations for the "combined" cases conform better. The reason is the influence from the hadron shells, which is more dominant for the universality than the cores [28, 41].

Compared with the 2 + 1-flavor model [22], we obtain nearly half of the masses of the stars from the present models, correspondingly with the half of the radii. Besides, the universal relations of the 2-flavor models seem to deviate from the referred NS model less than our previous work. The result reduces the mass gaps between NS and the QS in our previous work. We think the observations on the 2-flavor QS are able to supply the formation theories of the compact stars.

The ranges of the masses of the "simple" QS and "combined" cases enable these compact objects to emulate the observable properties of stellar-mass BH. The present study demonstrates that the I-Love-Q-C universal relations remain valid across a broad class of "combined" configurations, thereby reinforcing their applicability beyond 2-flavor quark matter systems. From an observational perspective, these universal relations may serve as a diagnostic tool to discriminate between BH and QS, particularly due to the vanishing TLN of BH in general relativity. Additionally, the observed deviations in compactness-related relations may offer potential insights into holographic quark matter models. Importantly, observations of "combined" QS could constrain the parameters governing the phase transition between deconfined quark matter and hadronic matter, thereby offering a pathway to probe the microphysics of dense matter in astrophysical environments.

#### 4 More Discussions on the $\epsilon$ and $p$ Parameter Space

In this section, we illustrate the whole  $\epsilon$  and  $p$  parameter space, and also consider a more complicated case study by replacing the previous simple conditions on  $\mu$  and  $T$  (as discussed in section 2) with a constant thermal conductivity constraint.

First, we numerically determine the relationships  $\epsilon(\mu, T)$  and  $p(\mu, T)$  using a holographic 2-flavor QCD model, presenting these correlations as heatmaps in Fig.7.

This visualization displays all the EoS information for the quark phase of holographic 2-flavor QCD model, expressing pressure  $p$  and energy density  $\epsilon$  as functions of chemical potential  $\mu$  and temperature  $T$ . The color gradient quantitatively indicates the values of these thermodynamic quantities. Our investigation concentrates solely on the quark-dominated regime situated above the first-order transition boundary. In the diagram, the shaded gray area corresponds to the hadronic matter domain, with both the CEP and first order line taken from reference [40].

Typically, realistic conditions assume rapid attainment of thermal equilibrium, corresponding to the constant-temperature stellar scenario already addressed in the preceding discussion of  $T = \text{constant}$ . We now turn to the next simplest non-trivial configuration - a stellar body with constant thermal conductivity and contain a thermal reservoir in the center, which will be our focus in the following analysis.

Although theoretically the thermal conductivity of each point in the  $(\mu, T)$  parameter space could be derived from holographic principles, we defer the complete holographic analysis to future work. For computational simplicity, we instead solve the TOV equations

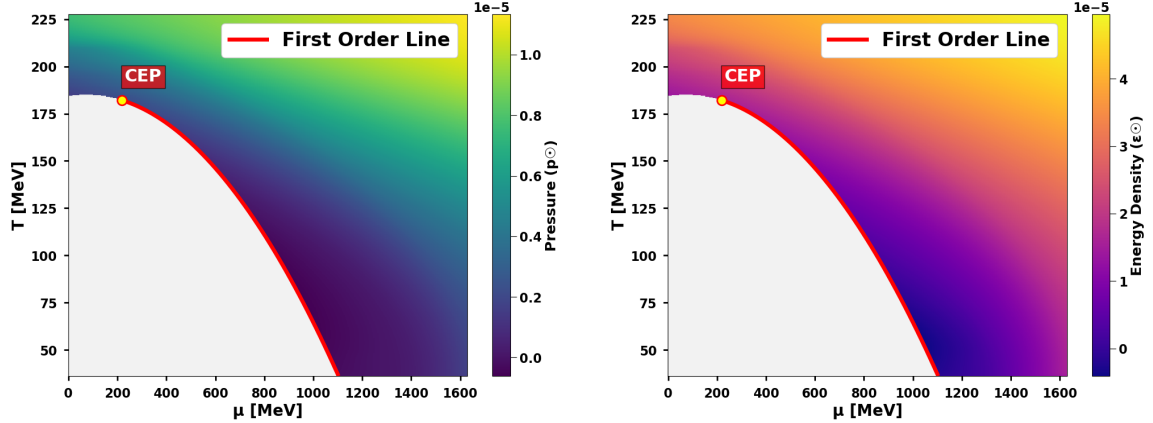


**Figure 7:** The heatmap presents all the  $T$ ,  $\mu$  dependence for  $p$  and  $\epsilon$  of the Holographic 2-flavor QCD Model (Notice that here for  $p$  and  $\epsilon$  we are using astronomical units  $p_{\odot}$  and  $\epsilon_{\odot}$  for later convenience, rather than QCD units):  $p = p(\mu, T)$  and  $\epsilon = \epsilon(\mu, T)$ , where the shading of the background color represents the magnitudes of  $p$  and  $\epsilon$ . The CEP and first order line are taken from reference [40].

starting from static field equations under constant thermal conductivity conditions. The temperature profile of QS is combined with the  $\mu$ - and  $T$ -dependent expressions of energy density ( $\epsilon$ ) and pressure ( $p$ ) to obtain solutions, followed by a discussion of key results.

The temperature distribution in stars with constant thermal conductivity satisfies the Laplace equation:

$$\nabla^2 T = 0. \quad (4.1)$$

Under assumptions of spherical symmetry, the solution takes the form  $T = C/R$ . However, this formulation does not yield a finite central temperature. To resolve this divergence, we introduce a cutoff at radius  $R = R_c$ , establishing the temperature profile:

$$T(r) = \begin{cases} T_0 & r \leq R_c \\ \frac{T_0 R_c}{r} & r > R_c. \end{cases} \quad (4.2)$$

Here, we suppose that the core region ( $r \leq R_c$ ) contains a constant-temperature heat source where the temperature field isn't governed by the Laplace equation.

Substituting  $T(r)$  into  $p(\mu, T)$  yields  $\mu(p, r)$ , which when combined with  $\epsilon(T, \mu)$  produces  $\epsilon(p, r)$ . This relationship serves as the EoS for TOV equation integration.

Fig.8a Shows the evolutionary paths of  $\mu(T)$  under TOV equation integration for different central initial conditions  $(\mu_0, T_0)$  near the phase transition boundary with  $R_c = 30$  km and 40 km. The pentagrams denote the integration starting points (stellar centers), while the crosses mark the termination points at the phase transition interface.

Notably, different initial conditions lead to distinct integration paths. Which means that our approach differs fundamentally from classical solutions as the EoS becomes dependent on central temperature  $T_0$ . Consequently, each QS requires a unique EoS, rendering traditional NS analysis methods (e.g., M-R curve stability criteria) inapplicable here.

We further investigate the  $R_c \rightarrow 0$  limit to eliminate core effects in Fig.8b. In this regime, the quark phase radius contracts proportionally with  $R_c$ , leading to constant pressure where  $\mu(T)$  reduces to an isobaric curve. Remarkably, sufficiently compact stars exhibit pressure-dominated behavior regardless of thermal profile, rendering the constant thermal conductivity condition trivial in this limit.

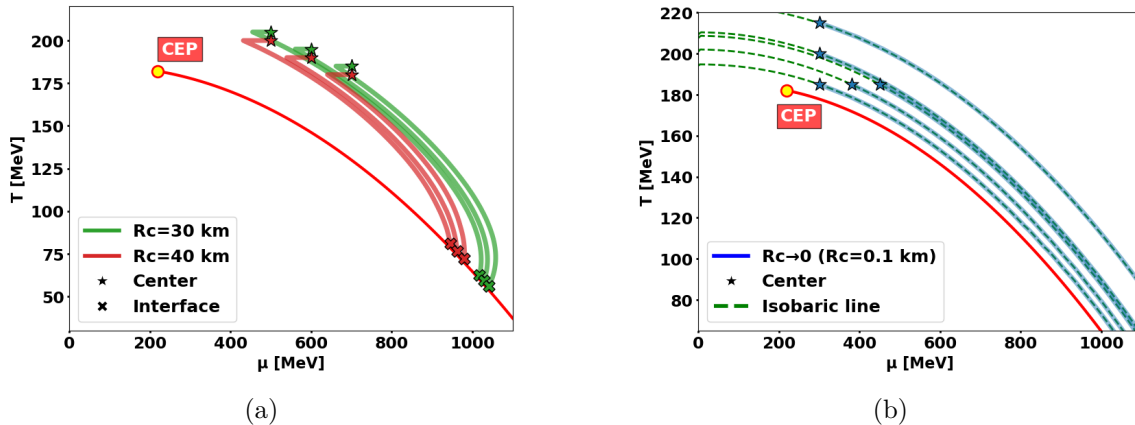


**Figure 8:** Paths of chemical potential and temperature  $(\mu, T)$  as functions of radius for different thermal core radius  $R_c$ : **(a)** Finite thermal core radius: As radius  $r$  increases, the path intersects the phase transition line and terminates at the stellar interface. Different central conditions  $(\mu_0, T_0)$  correspond to distinct trajectories, reflecting variations in the stellar EoS. **(b)** Infinitesimal core ( $R_c \rightarrow 0$ ): The pressure remains approximately constant during radial expansion, resulting in an isobaric trajectory.

For physical QS, the central temperature  $T_0$  and chemical potential  $\mu_0$  must satisfy constraints derived from matching to hadron phase exteriors. We adopt the same method as above by connecting to the external hadron shell EoS  $\epsilon_n = \kappa_n p^{\gamma_n}$  (with  $\gamma_n = 0.5$ ) beyond the phase transition boundary.

Fig.9 presents radial profiles of physical quantities for a single star of complete QS model with  $R_c = 10$  km and central parameters  $(T_0, \mu_0) = (200 \text{ MeV}, 500 \text{ MeV})$ . For simplicity, but enough to illustrate the idea, we select the case with an energy density jump factor of  $m = 1$ , which implies that the energy density is continuous at the phase transition. Then the constructed QS has the quark core radius  $R_t \approx 53$  km, and the total radius is 128 km, while the total mass is  $12.7 M_\odot$ , indeed well within the range spanned by the 5 different EoS cases in section 2.

**(a)-(c)** Radial profiles of pressure, cumulative mass, and energy density. The blue dashed curves denote contributions from the external hadron shell. Due to the imposed energy density jump factor  $m = 1$  at the interface, both pressure and cumulative mass remain smooth across the phase transition boundary. Discontinuities in derivatives of the energy density occur at  $R_c$  and the phase transition interface.

**(d)-(e)** Illustrate the radial profiles of temperature  $T$  and chemical potential  $\mu$  within the star. The temperature  $T$  strictly follows the distribution of (4.2). We truncate our calculations of  $T$  and  $\mu$  at the interface  $R_t$ , since the EoS of the external hadronic phase is

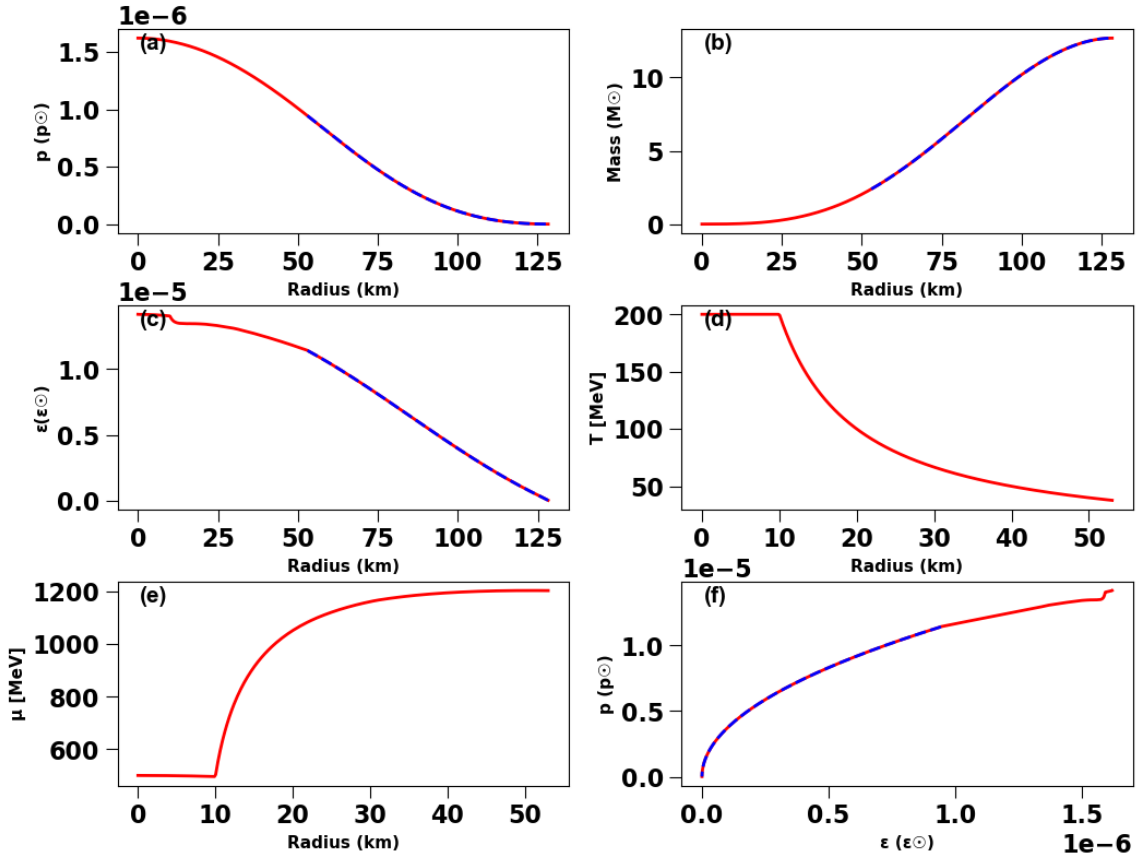


**Figure 9:** Radial profiles of physical quantities for a complete QS model with  $R_c = 10$  km and central parameters  $(T_0, \mu_0) = (200 \text{ MeV}, 500 \text{ MeV})$ . (a) Pressure, (b) Mass accumulation, (c) Energy density, (d) Temperature, (e) Chemical potential, and (f) EoS. Blue dashed curves denote contributions from the external single-polytropic hadron matter EoS with  $\gamma_n = 0.5$ .

described by a simple single polytrope, where the dependencies of  $T$  and  $\mu$  are not explicitly assigned.

Within  $R_c$ , the temperature is uniform, but the chemical potential  $\mu$  decreases along the constant  $T_0$  line due to the pressure gradient term in the TOV equations. Beyond  $R_c$ ,  $\mu$  initially increases but slightly decreases near the interface, intersecting the phase transition line.

(f) EoS of the star showing  $p(\epsilon)$  at different radii. The blue segment corresponds to the external single-polytropic NS EoS.

Under the condition of constant thermal conductivity, this section constructs the temperature- and chemical-potential-dependent EoS via a holographic two-flavor QCD model, and investigates the thermodynamic of QS through "combined" configurations with phase transition interfaces. Key findings highlight the unique EoS dependence on the central temperature  $T_0$  and the limiting behavior as  $R_c \rightarrow 0$ .

In the model of this section, to circumvent the divergence of the central temperature,



we introduced a central thermal core. However, we observed that its limiting case corresponds to a degenerate solution. Although the model yields an approximate well-behaved conclusion, more precise results should be derived from a holographic framework in future studies.

## 5 Conclusions

We extract the EoS for the 2-flavor quark-gluon plasma at high temperature using a holographic QCD model. Since the real EoS is a complicated function of chemical potential and temperature, we select five different cases combinations of  $\mu$  and  $T$  near CEP for simplified analysis and employ them as the core of QS, which would be enough to enclose the real EoS and offer a quick estimation for the possible range.

We first derive the M-R and the I-Love-Q-C relations with the "simple" 2-flavor quark EoS, which are analytical continuations of the fitting curves truncated at the phase transition points. Further to be more realistic and to make comparisons, we pay attention to "combined" QS: connecting the quark cores with polytropic hadron shells under different phase transitions and subsequently apply the "combined" cases to calculate the universal relations.

The results reveal that the mass distribution of both the "simple" and the "combined" QS are above  $2 M_{\odot}$ , which enable them to be BH mimickers. But the different wave forms and zero TLN of BH in the general relativity can help distinguish the QS from BH. The mass and radius combinations we obtain from the 2-flavor EoS are much different from those from the 2 + 1-flavor models [22], providing a method to infer the fundamental compositions of the hot QS. Compared with the NS, the I-Love-Q relations hold valid for the "simple" QS and the "combined" cases except for the  $m = 0.5$  model, extending the universal relations for both the continuous and the small discontinuous EoS. The relations about compactness deviate more from each model than the I-Love-Q relations, providing us an effective method to constrain the phenomenological models with phase transitions.

From Fig.2-6, it can be observed that quark stars exhibit a broad mass coverage spanning from about 2 to  $17 M_{\odot}$ , including the  $2.5\text{-}5 M_{\odot}$  range, which may effectively interpret the so-called mass gap. Another very interesting outcome is that, the minimum mass of QS (determined by the lowest pressure at the phase transition) approximates  $2 M_{\odot}$ . Below this threshold mass, hot QS would undergo phase transition to pure hot NS. This critical mass closely aligns with the upper mass limit of NS, which should not be a pure coincidence. Actually, this shows consistency with the results in the literature [12–16] that quark matter is not favored inside NS. If one want to get QS, the masses should exceed  $2 M_{\odot}$ , in addition to very high temperature. Unlike QS, hot NS lack a radiation-reflecting interface, leading to rapid cooling processes, and result in normal cold NS under  $2 M_{\odot}$ . This thermal characteristic could explain the observational absence of hot NS possessing radii as large as those predicted in our result.

An important new result of this work is presented in Fig.7, though not emphasized extensively, where we numerically determines all the  $T$ ,  $\mu$  dependence for  $p$  and  $\epsilon$  of the

quark phase in a holographic 2-flavor QCD model, presented as heatmaps spanning the entire parameter space.

Finally, we also discuss the temperature- and chemical-potential-dependent EoS under constant thermal conductivity with a heat source. Starting from the Laplace equation and combined with analysis of phase transition interfaces in QS, we reveal the thermodynamic properties of QS under this condition. It highlights the EoS dependence on the central temperature  $T_0$  and the limiting behavior as  $R_c \rightarrow 0$ , providing insights for potential future investigations.

*Acknowledgements.* The authors thank Song He, Chian-Shu Chen, Alessandro Parisi, Niko Jokela, Yi-Zhong Fan, Qiyuan Pan and Shao-Feng Ge for very helpful suggestions and discussions. KZ (Hong Zhang) is supported by a classified fund from Shanghai city.

## References

- [1] LIGO SCIENTIFIC, VIRGO collaboration, B. P. Abbott et al., *GW170817: Observation of Gravitational Waves from a Binary Neutron Star Inspiral*, *Phys. Rev. Lett.* **119** (2017) 161101, [[1710.05832](#)].
- [2] LIGO SCIENTIFIC, VIRGO collaboration, B. P. Abbott et al., *Properties of the binary neutron star merger GW170817*, *Phys. Rev. X* **9** (2019) 011001, [[1805.11579](#)].
- [3] LIGO SCIENTIFIC, VIRGO collaboration, B. P. Abbott et al., *GW190425: Observation of a Compact Binary Coalescence with Total Mass  $\sim 3.4M_\odot$* , *Astrophys. J. Lett.* **892** (2020) L3, [[2001.01761](#)].
- [4] T. Hinderer, *Tidal Love numbers of neutron stars*, *Astrophys. J.* **677** (2008) 1216–1220, [[0711.2420](#)].
- [5] M. C. Miller et al., *The Radius of PSR J0740+6620 from NICER and XMM-Newton Data*, *Astrophys. J. Lett.* **918** (2021) L28, [[2105.06979](#)].
- [6] E. Witten, *Anti-de sitter space, thermal phase transition, and confinement in gauge theories*, *arXiv preprint hep-th/9803131* (1998) .
- [7] J. Polchinski and M. J. Strassler, *The String dual of a confining four-dimensional gauge theory*, [hep-th/0003136](#).
- [8] G. W. Gibbons and K.-i. Maeda, *Black Holes and Membranes in Higher Dimensional Theories with Dilaton Fields*, *Nucl. Phys. B* **298** (1988) 741–775.
- [9] E. Witten, *Anti-de Sitter space, thermal phase transition, and confinement in gauge theories*, *Adv. Theor. Math. Phys.* **2** (1998) 505–532, [[hep-th/9803131](#)].
- [10] T. Sakai and S. Sugimoto, *Low energy hadron physics in holographic QCD*, *Prog. Theor. Phys.* **113** (2005) 843–882, [[hep-th/0412141](#)].
- [11] T. Sakai and S. Sugimoto, *More on a holographic dual of QCD*, *Prog. Theor. Phys.* **114** (2005) 1083–1118, [[hep-th/0507073](#)].
- [12] C. Hoyos, D. Rodríguez Fernández, N. Jokela and A. Vuorinen, *Holographic quark matter and neutron stars*, *Phys. Rev. Lett.* **117** (2016) 032501, [[1603.02943](#)].

- [13] C. Hoyos, N. Jokela, D. Rodríguez Fernández and A. Vuorinen, *Breaking the sound barrier in AdS/CFT*, *Phys. Rev. D* **94** (2016) 106008, [[1609.03480](#)].
- [14] E. Annala, C. Ecker, C. Hoyos, N. Jokela, D. Rodríguez Fernández and A. Vuorinen, *Holographic compact stars meet gravitational wave constraints*, *JHEP* **12** (2018) 078, [[1711.06244](#)].
- [15] K. Bitaghsir Fadafan, J. Cruz Rojas and N. Evans, *Deconfined, Massive Quark Phase at High Density and Compact Stars: A Holographic Study*, *Phys. Rev. D* **101** (2020) 126005, [[1911.12705](#)].
- [16] L. Zhang and M. Huang, *Holographic cold dense matter constrained by neutron stars*, *Phys. Rev. D* **106** (2022) 096028, [[2209.00766](#)].
- [17] K. Bitaghsir Fadafan, J. Cruz Rojas and N. Evans, *Holographic quark matter with colour superconductivity and a stiff equation of state for compact stars*, *Phys. Rev. D* **103** (2021) 026012, [[2009.14079](#)].
- [18] E. Annala, T. Gorda, A. Kurkela, J. Nättilä and A. Vuorinen, *Evidence for quark-matter cores in massive neutron stars*, *Nature Phys.* **16** (2020) 907–910, [[1903.09121](#)].
- [19] M.-Z. Han, Y.-J. Huang, S.-P. Tang and Y.-Z. Fan, *Plausible presence of new state in neutron stars with masses above  $0.98M_{\text{TOV}}$* , *Sci. Bull.* **68** (2023) 913–919, [[2207.13613](#)].
- [20] Y.-Z. Fan, M.-Z. Han, J.-L. Jiang, D.-S. Shao and S.-P. Tang, *Maximum gravitational mass  $M_{\text{TOV}}=2.25-0.07+0.08M_{\odot}$  inferred at about 3% precision with multimessenger data of neutron stars*, *Phys. Rev. D* **109** (2024) 043052, [[2309.12644](#)].
- [21] A. Kurkela, P. Romatschke and A. Vuorinen, *Cold Quark Matter*, *Phys. Rev. D* **81** (2010) 105021, [[0912.1856](#)].
- [22] L.-F. Chen, H.-Y. Yuan, M.-H. Zhou, K. Lu, J.-Y. Wu and K. Zhang, *Observing Hot Holographic Quark Star With Gravitational Waves*, [2501.17121](#).
- [23] R.-G. Cai, S. He, L. Li and Y.-X. Wang, *Probing QCD critical point and induced gravitational wave by black hole physics*, *Phys. Rev. D* **106** (2022) L121902, [[2201.02004](#)].
- [24] HOTQCD collaboration, A. Bazavov et al., *Equation of state in  $(2+1)$ -flavor QCD*, *Phys. Rev. D* **90** (2014) 094503, [[1407.6387](#)].
- [25] Y. Sekiguchi, K. Kiuchi, K. Kyutoku and M. Shibata, *Effects of hyperons in binary neutron star mergers*, *Phys. Rev. Lett.* **107** (2011) 211101, [[1110.4442](#)].
- [26] A. Drago and G. Pagliara, *The scenario of two families of compact stars: 2. Transition from hadronic to quark matter and explosive phenomena*, *Eur. Phys. J. A* **52** (2016) 41, [[1509.02134](#)].
- [27] K. Yagi and N. Yunes, *I-Love-Q*, *Science* **341** (2013) 365–368, [[1302.4499](#)].
- [28] K. Yagi and N. Yunes, *I-love-q relations in neutron stars and their applications to astrophysics, gravitational waves, and fundamental physics*, *Phys. Rev. D* **88** (Jul, 2013) 023009.
- [29] H. O. Silva and N. Yunes, *I-love-q to the extreme*, *Classical and Quantum Gravity* **35** (2017) .
- [30] C. Adam, A. G. Martín-Caro, M. Huidobro, R. Vázquez and A. Wereszczynski, *Quasiuniversal relations for generalized skyrme stars*, *Phys. Rev. D* **103** (Jan, 2021) 023022.
- [31] J. J. Li, A. Sedrakian and F. Weber, *Universal relations for compact stars with heavy baryons*, *Phys. Rev. C* **108** (2023) 025810, [[2306.14190](#)].

- [32] D. Atta, V. Singh and D. N. Basu, *Universal relationships for neutron stars from perturbative approach*, [2408.00646](#).
- [33] A. Kumar, M. K. Ghosh, P. Thakur, V. B. Thapa, K. K. Nath and M. Sinha, *Universal relations for compact stars with exotic degrees of freedom*, *Eur. Phys. J. C* **84** (2024) 692, [[2311.15277](#)].
- [34] P. Pani, *I-Love-Q relations for gravastars and the approach to the black-hole limit*, *Phys. Rev. D* **92** (2015) 124030, [[1506.06050](#)].
- [35] G. Martinon, A. Maselli, L. Gualtieri and V. Ferrari, *Rotating protoneutron stars: Spin evolution, maximum mass, and i-love-q relations*, *Physical Review D* **90** (Sept., 2014) .
- [36] S. Lau, P. Leung and L.-M. Lin, *Two-layer compact stars with crystalline quark matter: Screening effect on the tidal deformability*, *Physical Review D* **99** (Jan., 2019) .
- [37] A. R. Raduta, M. Oertel and A. Sedrakian, *Proto-neutron stars with heavy baryons and universal relations*, *Monthly Notices of the Royal Astronomical Society* **499** (Aug., 2020) 914–931.
- [38] P. Burikham, S. Pinkanjanarod and S. Ponglertsakul, *Slowly rotating neutron star with holographic multiquark core: I-love-q relations*, *Phys. Rev. D* **105** (May, 2022) 104018.
- [39] S. K. Roy and G. Chaudhuri, *I-c-q relations for rapidly rotating stable hybrid stars*, *Astroparticle Physics* **170** (2025) 103108.
- [40] Y.-Q. Zhao, S. He, D. Hou, L. Li and Z. Li, *Phase structure and critical phenomena in two-flavor QCD by holography*, *Phys. Rev. D* **109** (2024) 086015, [[2310.13432](#)].
- [41] J.-Y. Wu, W. Li, X.-H. Huang and K. Zhang, *Dark I-Love-Q*, [2309.07971](#).
- [42] K. Zhang, G.-Z. Huang, J.-S. Tsao and F.-L. Lin, *GW170817 and GW190425 as hybrid stars of dark and nuclear matter*, *Eur. Phys. J. C* **82** (2022) 366, [[2002.10961](#)].
- [43] D. W. Meltzer and K. S. Thorne, *Normal Modes of Radial Pulsation of Stars at the End Point of Thermonuclear Evolution*, *apj* **145** (Aug., 1966) 514.